ISSN 1070-3284, Russian Journal of Coordination Chemistry, 2016, Vol. 42, No. 2, pp. 104–115. © Pleiades Publishing, Ltd., 2016.
Original Russian Text © A.V. Ivanov, O.V. Loseva, T.A. Rodina, A.V. Gerasimenko, E.V. Novikova, 2016, published in Koordinatsionnaya Khimiya, 2016, Vol. 42, No. 2, pp. 91–102.

Gold(III)–Iron(III) Heteropolynuclear Complexes $([Au\{S_2CNR_2\}_2][FeCl_4])_n$ (R = C_4H_9, *iso*-C_4H_9): Chemisorption Synthesis, Supramolecular Self-Organization, and Thermal Behavior

A. V. Ivanov[a, *], O. V. Loseva[a], T. A. Rodina[b], A. V. Gerasimenko[c], and E. V. Novikova[d]

[a] *Institute of Geology and Nature Management, Far East Branch, Russian Academy of Sciences, Relochnyi per. 1, Blagoveshchensk, 675000 Russia*

[b] *Amur State University, sh. Ignat'eva 21, Blagoveshchensk, 675027 Russia*

[c] *Institute of Chemistry, Far East Branch, Russian Academy of Sciences, pr. Stoletiya Vladivostoka 159, Vladivostok, 690022 Russia*

[d] *Blagoveshchensk State Pedagogical University, ul. Lenina 104, Blagoveshchensk, 675000 Russia*

**e-mail: alexander.v.ivanov@chemist.com*

Received July 8, 2015

Abstract—The reactions of iron(III) dibutyl and di-*iso*-butyl dithiocarbamates $[Fe(S_2CNR_2)_3]$ (R = C_4H_9, *iso*-C_4H_9) with anions $[AuCl_4]^-$ in 2 M HCl are studied. The result of heterogeneous reactions of gold(III) chemisorption binding from a solution is the formation of gold(III)–iron(III) heteropolynuclear complexes of the ionic type. The crystal and supramolecular structures of polymer complexes $([Au\{S_2CN(C_4H_9)_2\}_2][FeCl_4])_n$ (**I**) and $([Au\{S_2CN(iso\text{-}C_4H_9)_2\}_2][FeCl_4])_n$ (**II**) are determined by X-ray diffraction analysis (CIF files CCDC 1407704 (**I**) and 1407802 (**II**)). The structure of complex **I** contains two centrosymmetrical structurally nonequivalent complex cations $[Au\{S_2CN(C_4H_9)_2\}_2]^+$ (**A** and **B**) and complex anion $[FeCl_4]^-$. Structure **II** is formed by three isomeric complex cations $[Au\{S_2CN(iso\text{-}C_4H_9)_2\}_2]^+$ (**A**, **B**, and **C**) and two anions $[FeCl_4]^-$ related as conformers. The isomeric cations are involved in the formation of linear $(\cdots\mathbf{A}\cdots\mathbf{B}\cdots)_n$ (in **I**) or zigzag $(\cdots\mathbf{A}\cdots\mathbf{B}\cdots\mathbf{A}\cdots\mathbf{C}\cdots)_n$ (in **II**) polymer chains due to pairs of weak secondary interactions Au···S. The thermal behavior of the complexes is studied by simultaneous thermal analysis. Thermal destruction includes the thermolysis of the dithiocarbamate moiety of the complexes and anions $[FeCl_4]^-$ with the reduction of gold(III), release of $FeCl_3$, and partial formation of Fe_2O_3. The final thermolysis products are metallic gold and Fe_2O_3.

DOI: 10.1134/S1070328416020032

INTRODUCTION

Coordination compounds of transition metals with dithiocarbamate ligands are interesting because of diverse areas of their practical application. They are used as polymerization initiators for the preparation of polystyrene and poly(methyl methacrylate) [1] and precursors in the preparation of nanosized powders of metal sulfides [2–6]. They manifest the properties of sensors to chemical volatiles [7] and luminophores [8, 9] and spin traps of nitrogen(II) oxide in biological systems [10]. The dithiocarbamate complexes exhibit catalytic [9, 11], antibacterial [12, 13], and anticancer activities [14–16]. In addition, the transition metal dithiocarbamates are characterized by the capability of chemisorption binding of gold(III) from solutions. The efficient character of gold(III) binding has earlier been established for dialkyl dithiocarbamates of a series of metals, which resulted in the formation of polymer heteronuclear complexes gold(III)–cadmium and gold(III)–zinc $([Au\{S_2CNR_2\}_2]_2X)_n$ (X = $[CdCl_4]^{2-}$, $[Cd_2Cl_6]^{2-}$, $[ZnCl_4]^{2-}$) [17–23], gold(III)–bismuth $([Au\{S_2CNR_2\}_2]_3X)_n$ (X = $[Bi_2Cl_9]^{3-}$, $[Bi_3Cl_{12}]^{3-}$) [24, 25], and gold(III)–thallium(III) $([Au\{S_2CN(iso\text{-}C_4H_9)_2\}_2][TlCl_4])_n$ [26] with a complicatedly organized supramolecular structure. Therefore, it was of interest to study the interaction of iron(III) dialkyl dithiocarbamates with solutions of gold(III), the synthesis of the gold(III)–iron(III) dithiocarbamate chloride complexes, and their structural organization and thermal behavior.

In this work, we studied the reactions of the iron(III) dialkyl dithiocarbamate complexes $[Fe(S_2CNR_2)_3]$ (R = C_4H_9, *iso*-C_4H_9) with gold(III) in acidic solutions. The heterogeneous reaction of gold(III) binding with freshly precipitated iron(III) dithiocarbamates is accompanied by the formation of new gold(III)–iron(III) heteropolynuclear complexes $([Au\{S_2CN(C_4H_9)_2\}_2][FeCl_4])_n$ (**I**) and $([Au\{S_2CN(iso\text{-}C_4H_9)_2\}_2][FeCl_4])_n$ (**II**). The crystal

and supramolecular structures of preparatively isolated complexes **I** and **II** were determined by X-ray diffraction analysis, and the thermal behavior was studied by simultaneous thermal analysis (STA).

EXPERIMENTAL

Sodium dibutyl and di-*iso*-butyl dithiocarbamates obtained by the reaction of carbon sulfide (Merck) with dibutyl- and di-*iso*-butylamine (Aldrich) in an alkaline medium were characterized by MAS ^{13}C NMR spectroscopy (δ, ppm).

$Na\{S_2CN(C_4H_9)_2\} \cdot H_2O$: 208.3 ($-S_2CN=$); 55.2 ($=NCH_2-$); 30.0, 21.0 ($-CH_2-$); 15.6, 14.9, 14.5 (2 : 1 : 1, $-CH_3$).

$Na\{S_2CN(iso\text{-}C_4H_9)_2\} \cdot 3H_2O$: 208.2 ($-S_2CN=$); 66.7 ($=NCH_2-$); 28.0, 27.1 (1 : 1, $-CH=$); 23.0, 22.4, 20.8 (1 : 1 : 2, $-CH_3$).

Iron(III) dialkyl dithiocarbamates were synthesized by the precipitation of Fe^{3+} ions from the aqueous phase with the corresponding sodium dithiocarbamates [27].

Synthesis of I and II. Polymeric bis(*N*,*N*-dibutyldithiocarbamato-S,S')gold(III) tetrachloroferrate(III) (**I**) and bis(*N*,*N*-di-*iso*-butyldithiocarbamato-S,S')gold(III) tetrachloroferrate(III) (**II**) were synthesized by the interaction of freshly precipitated $[Fe(S_2CNR_2)_3]$ (R = C_4H_9, *iso*-C_4H_9) with a solution of $AuCl_3$ in 2 M HCl. A solution (10 mL) of $AuCl_3$ (in 2 M HCl) containing of gold (28 mg) was poured to each black iron(III) dialkyl dithiocarbamate complex (100 mg), and the resulting solutions were stirred for 60 min. The residual gold content and iron content in the solution were determined on an atomic absorption spectrometer (class 1, model 180-50, Hitachi). The obtained black-brown precipitate was filtered off, washed with water, and dried on a filter. The heterogeneous binding of gold(III) from a solution by the precipitates of iron(III) dithiocarbamates accompanied by the formation of the gold(III)–iron(III) heteronuclear complexes of the ionic type includes the decomposition of one of three ligands

$$[Fe(S_2CNR_2)_3] + H[AuCl_4] = [Au(S_2CNR_2)_2][FeCl_4] + CS_2 + HNR_2.$$

Crystals of compounds **I** and **II** for X-ray diffraction analysis were obtained after the completion of their interaction with gold(III) by the dissolution of precipitates of the chemisorbing complexes in acetone followed by the slow evaporation of the solvent. Crystallization gave yellow prismatic (**I**) and plate-like (**II**) crystals.

X-ray diffraction analyses were carried out for single crystals of complexes **I** and **II** on BRUKER Kappa APEX2 and BRUKER Smart APEX2 diffractometers, respectively (MoK_α radiation, λ = 0.71073 Å, graphite monochromator) at 170(1) and 200(2) K. The X-ray experiment for complex **I** was carried out from a twin crystal at a crystal–detector distance of 50 mm. Two domains are turned relatively to each other by 180° about the reciprocal vector [0 1 1]*. The first domain gave 30147 reflections (6585 independent reflections). The second domain gave 29553 reflections (6459 independent reflections). Two domains gave 11825 overlapped reflections (3120 independent reflections). The final structure refinement was performed by the experimental data for the first domain. The BASF parameter refined in the SHELXTL/PC programs was equal to 0.073(1). Structure **II** was determined by a direct method and refined by the least-squares method in the anisotropic approximation of non-hydrogen atoms. An X-ray absorption correction was applied by equivalent reflections. For both **I** and **II**, the positions of hydrogen atoms were calculated geometrically and included in the refinement by the riding model. Data were collected and edited and the unit cell parameters were refined using the APEX2 [28] and SAINT [29] programs. All calculations on structure determination and refinement were performed using the SHELXTL/PC programs [30]. The main crystallographic data and the refinement results for structures **I** and **II** are presented in Table 1. Selected bond lengths and angles are given in Table 2.

The coordinates of atoms, bond lengths, and bond angles were deposited with the Cambridge Crystallographic Data Centre (CIF files 1407704 (**I**) and 1407802 (**II**); deposit@ccdc.cam.ac.uk or http://www.ccdc.cam.ac.uk).

Thermal behavior was studied by the STA method including the simultaneous detection of thermogravimetry (TG) and differential scanning calorimetry (DSC) curves. The study was carried out on an STA 449C Jupiter instrument (NETZSCH) in corundum crucibles under caps with a hole providing a vapor pressure of 1 atm for the thermal decomposition of the sample. The heating rate was 5°C/min to 1250°C in argon. The samples were recorded additionally in aluminum crucibles to reveal thermal effects more distinctly. The weighed samples were 4.120–4.443 mg, the accuracy of temperature measurement was ±1°C, and that of weight change was $\pm 1 \times 10^{-4}$ mg.

After thermal analysis, the residual substance was examined on a JSM-35C JEOL analytical scanning electron microscope equipped with a 35-SDS type wave dispersive spectrometer (a secondary electron image was used). The chemical composition was determined qualitatively using the microprobe method on a RONTEC energy dispersive spectrometer integrated with a LEO-1420 scanning electron microscope.

RESULTS AND DISCUSSION

The unit cells of compounds **I** and **II** include two and eight formula units $[Au(S_2CNR_2)_2][FeCl_4]$ (R =

Table 1. Crystallographic data, experimental details, and refinement parameters for structures **I** and **II**

Parameter	Value	
	I	**II**
Empirical formula	$C_{18}H_{36}N_2S_4Cl_4FeAu$	$C_{18}H_{36}N_2S_4Cl_4FeAu$
FW	803.34	803.34
Crystal system	Triclinic	Monoclinic
Space group	$P\bar{1}$	$P2_1/n$
a, Å	9.9057(2)	15.6551(6)
b, Å	11.7770(3)	15.0235(6)
c, Å	13.0598(3)	26.233(1)
α, deg	79.2320(10)	90
β, deg	89.8080(10)	96.717(1)
γ, deg	84.8800(10)	90
V, Å^3	1490.61(6)	6127.6(4)
Z	2	8
ρ_{calcd}, g/cm^3	1.790	1.742
μ, mm^{-1}	6.051	5.888
F(000)	790	3160
Crystal size, mm	0.20 × 0.11 × 0.05	0.34 × 0.20 × 0.07
Data collection for θ range, deg	1.59–28.00	1.44–31.27
Ranges of reflection indices	$-13 \leqslant h \leqslant 13$, $-15 \leqslant k \leqslant 15$, $0 \leqslant l \leqslant 17$	$-22 \leqslant h \leqslant 22$, $-21 \leqslant k \leqslant 21$, $-37 \leqslant l \leqslant 24$
Measured reflections	71525	48960
Independent reflections	7196	18437 ($R_{int} = 0.0321$)
Reflections with $I > 2\sigma(I)$	5820	14527
Refinement parameters	279	639
Goodness-of-fit	1.085	1.002
R factors for $F^2 > 2\sigma(F^2)$	$R_1 = 0.0335$, $wR_2 = 0.0840$	$R_1 = 0.0309$, $wR_2 = 0.0601$
R factors for all reflections	$R_1 = 0.0482$, $wR_2 = 0.0907$	$R_1 = 0.0475$, $wR_2 = 0.0648$
Residual electron density (min/max), *e*/Å^3	−2.517/0.774	−0.955/0.929

C_4H_9, *iso*-C_4H_9), respectively (Figs. 1 and 2). Complexes **I** and **II** contain structurally nonequivalent complex cations $[Au\{S_2CNR_2\}_2]^+$: two cations in **I** (R = C_4H_9) and three cations in **II** (R = *iso*-C_4H_9). The cationic moiety of compound **I** is presented by two isomeric centrosymmetrical cations $[Au\{S_2CN(C_4H_9)_2\}_2]^+$ including the Au(1) and Au(2) atoms (hereinafter, cations **A** and **B**, Fig. 3a). In turn, complex **II** contains noncentrosymmetrical cation **A** with the Au(1) atom and centrosymmetrical cations **B** and **C** with the Au(2) and Au(3) atoms, respectively (Fig. 4). In each complex cation, the gold atom coordinates two Dtc ligands through the S,S'-bidentate mode. The coordination mode of the ligands is nearly isobidentate: the maximum difference in Au–S bond lengths is 0.01 Å. In noncentrosymmetrical cation **A** of complex **II**, one of the Dtc ligands is noticeably more strongly bound to the Au atom than the second ligand (Table 2). The coordination of two Dtc ligands by gold leads to the formation of a bicyclic system $[CS_2AuS_2C]$ with the metal atom in the *spiro* position. Small sizes of the four-membered metallocycles $[AuS_2C]$ are illustrated by the interatomic distances Au···C 2.831–2.848 Å and S···S 2.840–2.856 Å, which are significantly smaller than the sum of the van der Waals radii of the corresponding pairs of atoms: 3.36 and 3.60 Å [31, 32]. Thus, the positions of the gold and carbon atoms in the discussed metallocycles are substantially brought together, indicating the direct *trans*-annular interaction between them and a high concentration of the π-electron density delocalized inside the cycles. The $[AuS_2C]$ groups are almost planar, and the AuSSC and AuSCS torsion angles are close to 180° (Table 2). The mutual arrangement of the discussed atoms in cations **B** and **C** (structure **II**) deviates from the coplanar arrangement due to tetrahedral distortion. The geometry of the chromophores $[AuS_4]$ is

Table 2. Selected bond lengths (*d*) and bond (ω) and torsion (φ) angles in structures **I** and **II***

Compound **I**			
Cation **A**		Cation **B**	
Bond	*d*, Å	Bond	*d*, Å
Au(1)–S(1)	2.3328(11)	Au(2)–S(3)	2.3408(13)
Au(1)–S(2)	2.3369(11)	Au(2)–S(4)	2.3329(13)
Au(1)···S(3)	3.6869(13)	Au(2)···S(2)[a]	3.8600(12)
S(1)–C(1)	1.724(5)	S(3)–C(10)	1.737(5)
S(2)–C(1)	1.741(4)	S(4)–C(10)	1.729(5)
N(1)–C(1)	1.297(6)	N(2)–C(10)	1.297(6)
N(1)–C(2)	1.479(6)	N(2)–C(11)	1.469(7)
N(1)–C(6)	1.485(6)	N(2)–C(15)	1.472(7)
Angle	ω, deg	Angle	ω, deg
S(1)Au(1)S(2)	72.26(4)	S(3)Au(2)S(4)	75.33(5)
C(1)S(1)Au(1)	87.2(2)	C(10)S(3)Au(2)	86.6(2)
C(1)S(2)Au(1)	86.7(2)	C(10)S(4)Au(2)	87.03(2)
S(1)C(1)S(2)	110.7(2)	S(3)C(10)S(4)	110.9(3)
N(1)C(1)S(1)	124.9(3)	N(2)C(10)S(3)	125.1(4)
N(1)C(1)S(2)	124.4(4)	N(2)C(10)S(4)	124.0(4)
Angle	φ, deg	Angle	φ, deg
Au(1)S(1)S(2)C(1)	−178.2(2)	Au(2)S(3)S(4)C(10)	176.2(3)
S(1)Au(1)C(1)S(2)	−178.4(2)	S(3)Au(2)C(10)S(4)	176.6(3)
S(1)C(1)N(1)C(2)	−179.6(3)	S(3)C(10)N(2)C(11)	1.1(7)
S(1)C(1)N(1)C(6)	−1.0(6)	S(3)C(10)N(2)C(15)	−177.3(4)
S(2)C(1)N(1)C(2)	0.3(6)	S(4)C(10)N(2)C(11)	−178.9(4)
S(2)C(1)N(1)C(6)	178.9(3)	S(4)C(10)N(2)C(15)	2.7(7)
Anion			
Bond	*d*, Å	Bond	*d*, Å
Fe–Cl(1)	2.174(2)	Fe–Cl(3)	2.180(2)
Fe–Cl(2)	2.183(2)	Fe–Cl(4)	2.193(2)
Angle	ω, deg	Angle	ω, deg
Cl(1)FeCl(2)	110.80(9)	Cl(2)FeCl(4)	109.99(8)
Cl(1)FeCl(3)	111.24(8)	Cl(3)FeCl(2)	107.97(7)
Cl(1)FeCl(4)	108.87(8)	Cl(3)FeCl(4)	107.92(8)
Compound **II**			
Cation **A**			
Bond	*d*, Å	Bond	*d*, Å
Au(1)–S(1)	2.3398(7)	S(3)–C(10)	1.730(3)
Au(1)–S(2)	2.3498(7)	S(4)–C(10)	1.735(3)
Au(1)–S(3)	2.3282(7)	N(1)–C(1)	1.312(3)
Au(1)–S(4)	2.3316(7)	N(1)–C(2)	1.477(4)
Au(1)···S(6)	3.6857(8)	N(1)–C(6)	1.482(3)
Au(1)···S(7)	3.6824(8)	N(2)–C(10)	1.304(3)
S(1)–C(1)	1.732(3)	N(2)–C(11)	1.476(3)
S(2)–C(1)	1.733(3)	N(2)–C(15)	1.484(3)

Table 2. (Contd.)

Compound **II**			
Cation **A**			
Angle	ω, deg	Angle	ω, deg
S(1)Au(1)S(2)	75.01(2)	C(10)S(3)Au(1)	87.51(9)
S(1)Au(1)S(3)	104.26(2)	C(10)S(4)Au(1)	87.29(9)
S(1)Au(1)S(4)	176.61(3)	S(1)C(1)S(2)	111.0(2)
S(2)Au(1)S(3)	177.91(3)	S(3)C(10)S(4)	110.09(14)
S(2)Au(1)S(4)	105.74(2)	N(1)C(1)S(1)	124.0(2)
S(3)Au(1)S(4)	75.10(2)	N(1)C(1)S(2)	125.0(2)
C(1)S(1)Au(1)	87.18(9)	N(2)C(10)S(3)	125.0(2)
C(1)S(2)Au(1)	86.82(9)	N(2)C(10)S(4)	124.9(2)
Angle	φ, deg	Angle	φ, deg
Au(1)S(1)S(2)C(1)	178.2(2)	Au(1)S(3)S(4)C(10)	−179.3(2)
S(1)Au(1)C(1)S(2)	178.4(1)	S(3)Au(1)C(10)S(4)	−179.4(1)
S(1)C(1)N(1)C(2)	−4.0(4)	S(3)C(10)N(2)C(11)	170.1(2)
S(1)C(1)N(1)C(6)	178.8(2)	S(3)C(10)N(2)C(15)	−8.0(4)
S(2)C(1)N(1)C(2)	175.2(2)	S(4)C(10)N(2)C(11)	−9.5(4)
S(2)C(1)N(1)C(6)	−2.0(4)	S(4)C(10)N(2)C(15)	172.5(2)
Cation **B**		Cation **C**	
Bond	*d*, Å	Bond	*d*, Å
Au(2)−S(5)	2.3349(7)	Au(3)−S(7)	2.3409(7)
Au(2)−S(6)	2.3355(7)	Au(3)−S(8)	2.3364(7)
Au(2)···S(1)	3.6103(8)	Au(3)···S(2)	3.5893(8)
S(5)−C(19)	1.730(3)	S(7)−C(28)	1.743(3)
S(6)−C(19)	1.736(3)	S(8)−C(28)	1.736(3)
N(3)−C(19)	1.302(3)	N(4)−C(28)	1.301(3)
N(3)−C(24)	1.471(3)	N(4)−C(29)	1.476(3)
N(3)−C(20)	1.476(4)	N(4)−C(33)	1.482(3)
Angle	ω, deg	Angle	ω, deg
S(5)Au(2)S(6)	75.15(2)	S(7)Au(3)S(8)	75.08(2)
C(19)S(5)Au(2)	87.14(9)	C(28)S(7)Au(3)	87.14(9)
C(19)S(6)Au(2)	87.00(10)	C(28)S(8)Au(3)	87.44(9)
S(5)C(19)S(6)	110.5(2)	S(7)C(28)S(8)	110.1(2)
N(3)C(19)S(5)	124.9(2)	N(4)C(28)S(7)	124.9(2)
N(3)C(19)S(6)	124.6(2)	N(4)C(28)S(8)	125.0(2)
Angle	φ, deg	Angle	φ, deg
Au(2)S(5)S(6)C(19)	174.7(2)	Au(3)S(7)S(8)C(28)	−174.1(2)
S(5)Au(2)C(19)S(6)	175.2(2)	S(7)Au(3)C(28)S(8)	−174.7(1)
S(5)C(19)N(3)C(20)	−173.0(2)	S(7)C(28)N(4)C(29)	2.7(4)
S(5)C(19)N(3)C(24)	2.4(4)	S(7)C(28)N(4)C(33)	179.4(2)
S(6)C(19)N(3)C(20)	6.0(4)	S(8)C(28)N(4)C(29)	−175.4(2)
S(6)C(19)N(3)C(24)	−178.5(2)	S(8)C(28)N(4)C(33)	1.3(4)
Anion **D**		Anion **E**	
Bond	*d*, Å	Bond	*d*, Å
Fe(1)−Cl(1)	2.1957(8)	Fe(2)−Cl(5)	2.1919(13)
Fe(1)−Cl(2)	2.2001(10)	Fe(2)−Cl(6)	2.1874(9)

Table 2. (Contd.)

Compound **II**			
Anion **D**		Anion **E**	
Bond	*d*, Å	Bond	*d*, Å
Fe(1)–Cl(3)	2.1942(10)	Fe(2)–Cl(7)	2.1817(11)
Fe(1)–Cl(4)	2.1867(10)	Fe(2)–Cl(8)	2.1992(11)
Angle	ω, deg	Angle	ω, deg
Cl(1)Fe(1)Cl(2)	107.57(4)	Cl(5)Fe(2)Cl(6)	109.47(5)
Cl(1)Fe(1)Cl(3)	109.86(4)	Cl(5)Fe(2)Cl(7)	110.83(6)
Cl(1)Fe(1)Cl(4)	109.30(4)	Cl(5)Fe(2)Cl(8)	109.64(6)
Cl(2)Fe(1)Cl(3)	110.73(4)	Cl(6)Fe(2)Cl(7)	109.72(4)
Cl(2)Fe(1)Cl(4)	109.95(4)	Cl(6)Fe(2)Cl(8)	108.48(4)
Cl(3)Fe(1)Cl(4)	109.40(4)	Cl(7)Fe(2)Cl(8)	108.66(4)

* Symmetry transforms: [a] $-x + 1, -y + 1, -z + 2$ (**I**).

close to the planar tetrahedral one with the low-spin (inner-orbital) dsp^2-hybrid state of the gold(III) atom.

The anionic moiety of complexes **I** and **II** is presented by ions $[FeCl_4]^-$, in each of which the central iron atom (sp^3-hybridization state) exists in the distorted tetrahedral environment of four structurally nonequivalent chlorine atoms (Fe–Cl 2.174–2.2001 Å, angles ClFeCl 107.57°–111.24°). The structure of complex **II** includes two isomeric $[FeCl_4]^-$ anions **D** and **E** with the Fe(1) and Fe(2) atoms, respectively (Fig. 5b, Table 2). The character of differences between the respective structural characteristics of the nonequivalent gold(III) cations and iron(III) anions (Table 2) makes it possible to classify them as conformational isomers.

The supramolecular self-organization of complexes **I** and **II** occurs by relatively weak secondary bonds[1] Au···S of the nonvalent type between the complex cations. In compound **I**, each of isomeric cations **A** and **B** forms two pairs of these nonsymmetrical bonds with the neighbors: Au(1)···S(3) and Au(1)···S(3)[b] 3.6869; Au(2)···S(2)[a] and Au(2)···S(2)[e] 3.8600 Å, due to which linear polymer chains $[\cdots\mathbf{A}\cdots\mathbf{B}\cdots]_n$ oriented along the crystallographic axis *x* are formed (Fig. 3a). The length of the discussed bonds exceeds the sum of the van der Waals radii of gold and sulfur (3.46 Å) [31, 32]. The Au(1)···Au(2)

[1] The concept of secondary bonds was proposed [33] for the description of interactions characterized by the distances comparable with the sums of the van der Waals radii of the corresponding atoms.

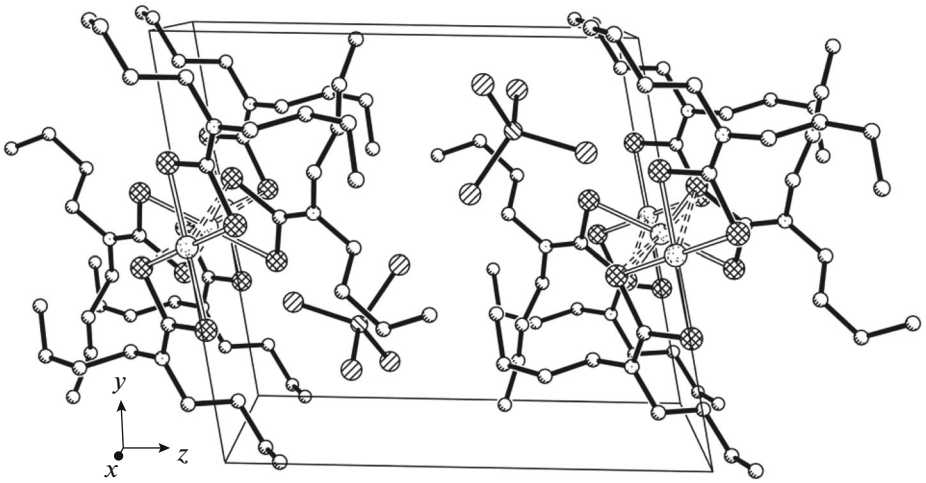

Fig. 1. Perspective view of the structure $([Au\{S_2CN(C_4H_9)_2\}_2][FeCl_4])_n$ (**I**) along the axis *x*.

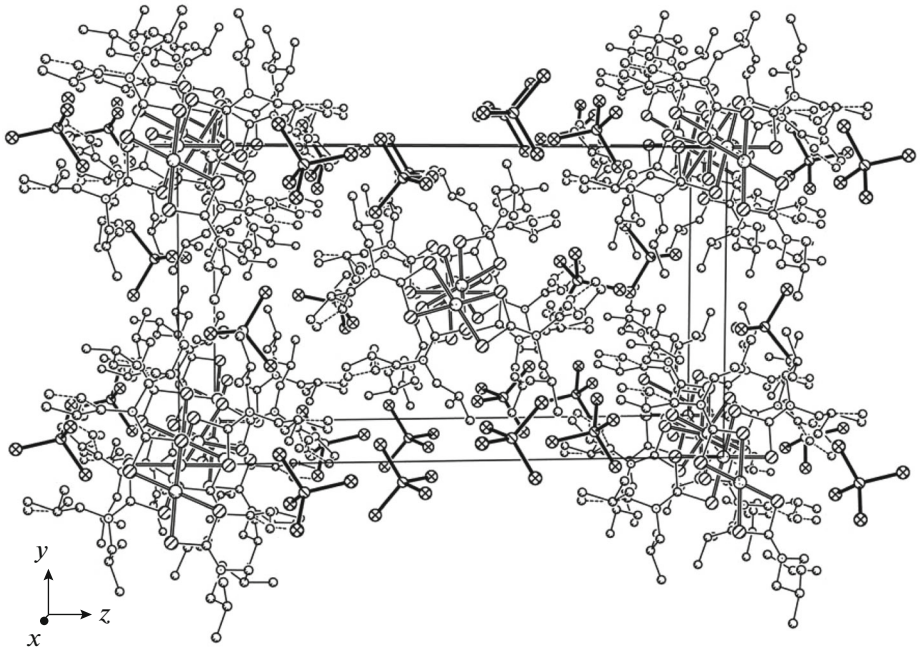

Fig. 2. Perspective view of the structure $([Au\{S_2CN(iso\text{-}C_4H_9)_2\}_2][FeCl_4])_n$ (**II**) along the axis *x*.

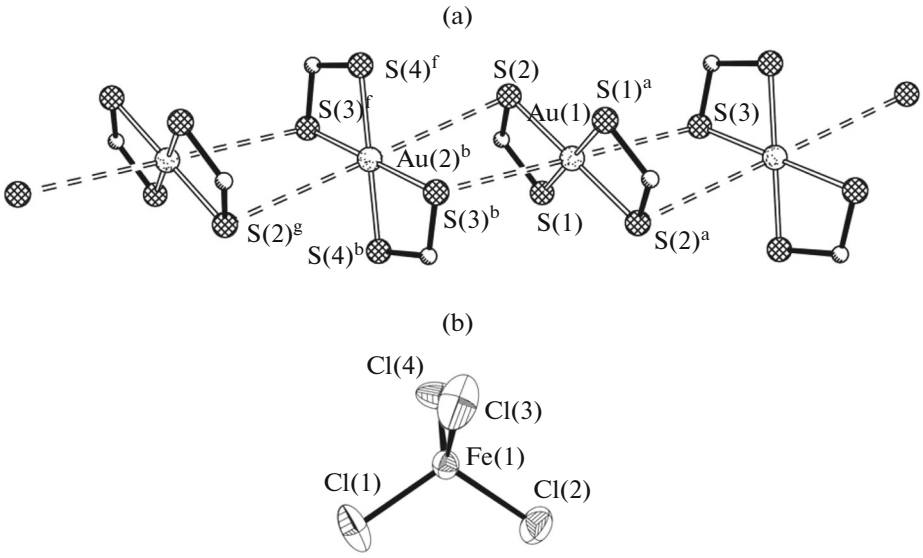

Fig. 3. (a) Fragment of the cationic polymer chain $([Au\{S_2CN(C_4H_9)_2\}_2]^+)_n$ in complex **I** and (b) the tetrahedral anion $[FeCl_4]^-$.

distance in the polymer chain is 4.953 Å. The $[FeCl_4]^-$ anions alternate at the right and left from the polymer chains (Figs. 1 and 3b). It follows from the structural fragment shown in Fig. 3a that in each gold(III) cation only two diagonally oriented sulfur atoms are involved in secondary binding: the atoms S(2) in cation **A** and S(3) in cation **B** (Table 2).

More complicatedly organized supramolecular structure **II** is caused by the presence of three isomeric gold(III) complex cations and two isomeric iron(III) anions. All cations $[Au\{S_2CN(iso\text{-}C_4H_9)_2\}_2]^+$ are involved in the construction of the polymer chain due to pairs of nonsymmetrical Au···S bonds. However, in nonsymmetrical cation **A**, the sulfur atoms of only one Dtc ligand, S(1) and S(2), are involved in binding, whereas cations **B** and **C** present for binding the diagonally oriented atoms S(6), $S(6)^b$ and S(7), $S(7)^a$, respectively (Fig. 4, Table 2). Four nonequivalent

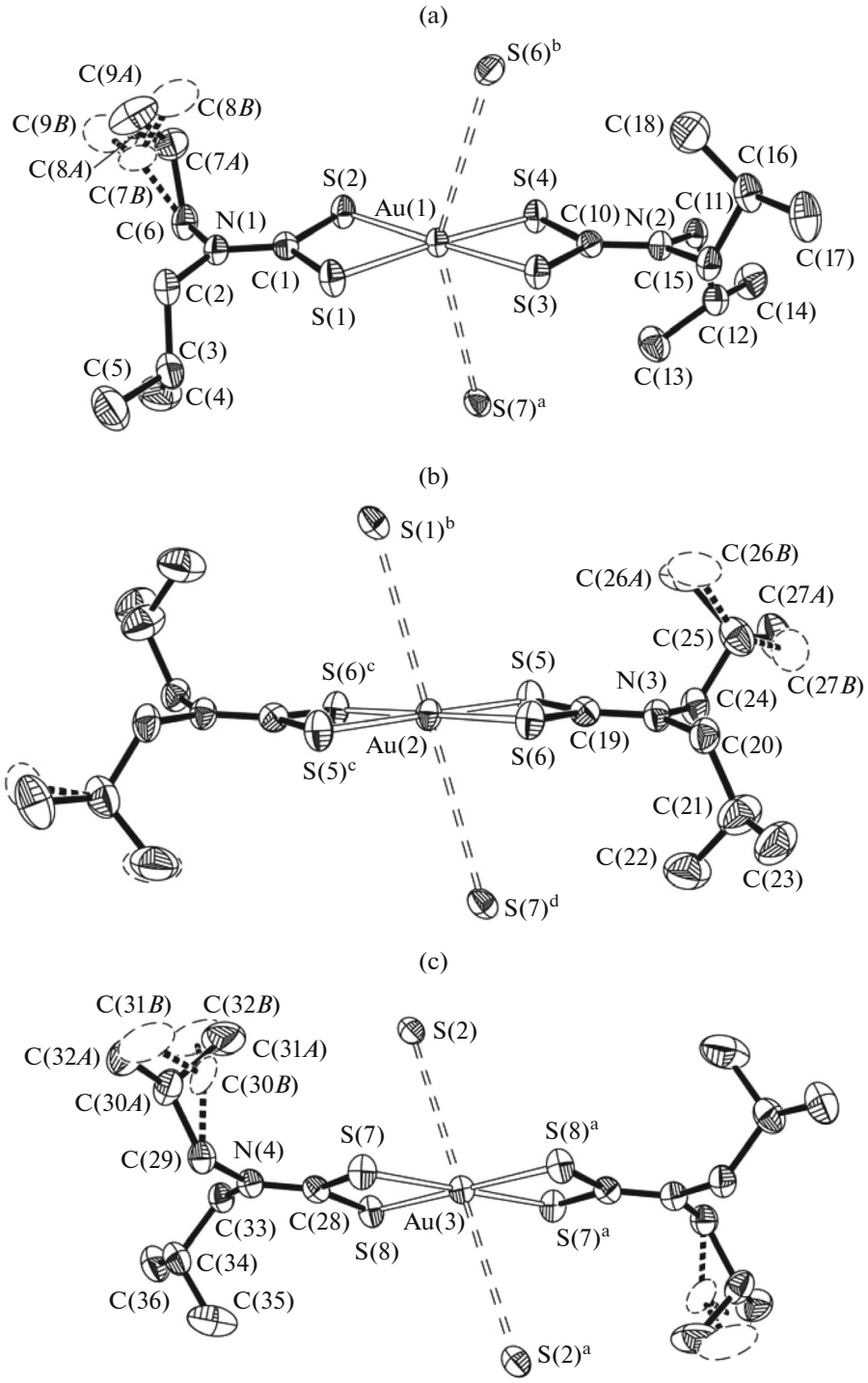

Fig. 4. Structures of isomeric complex cations (a) **A**, (b) **B**, and (c) **C** of compound **II**. Ellipsoids of 50% probability.

Au···S bonds are observed between the adjacent isomeric cations $[Au\{S_2CN(iso\text{-}C_4H_9)_2\}_2]^+$: Au(1)···S(6) 3.6857, Au(1)···S(7) 3.6824, Au(2)···S(1) 3.6103, and Au(3)···S(2) 3.5893 Å. The bonds result in the formation of zigzag supramolecular chains $[\cdots\mathbf{A}\cdots\mathbf{B}\cdots\mathbf{A}\cdots\mathbf{C}\cdots]_n$ (Fig. 5a). The distances are Au(1)···Au(2) 3.933 and Au(1)···Au(3) 4.018 Å, and the Au(2)Au(1)Au(3) angle is 159.76°. In addition, the isomeric gold(III) complex cations in polymer chains of compounds **I** and **II** are characterized by different spatial orientations (Figs. 3a and 5a).

The presence of secondary interactions in the polymer chains results in the formation of extended distorted octahedral chromophores $[AuS_6]$ by each gold

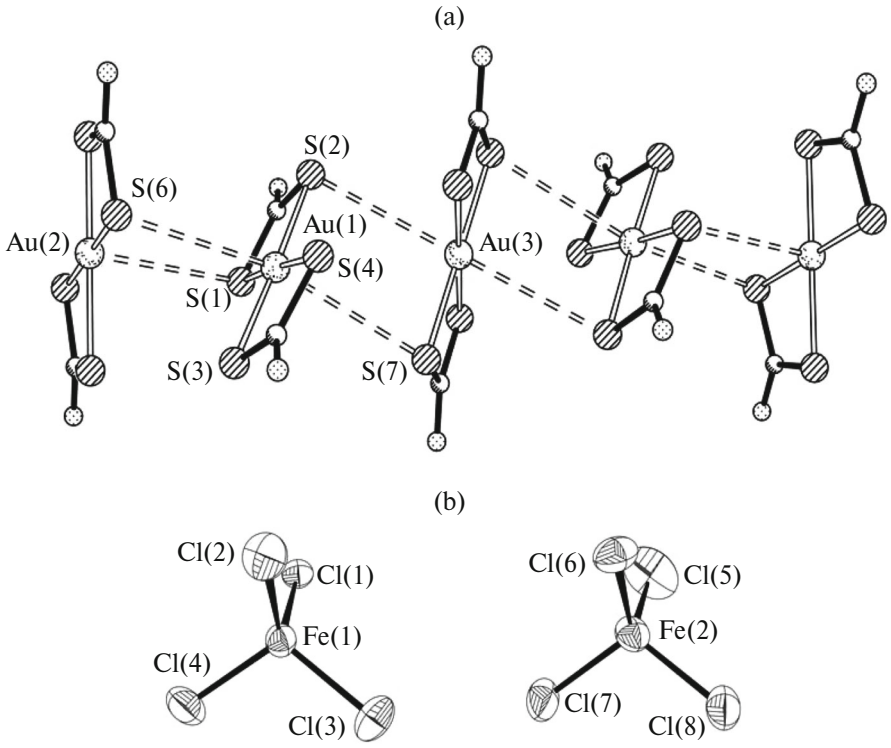

Fig. 5. (a) Fragment of the cationic polymer chain $([Au\{S_2CN(iso\text{-}C_4H_9)_2\}_2]^+)_n$ in complex **II** and (b) the isomeric anions $[FeCl_4]^-$. Ellipsoids of 50% probability.

atom. It should be mentioned that the sulfur atoms, which are not involved in the secondary interactions Au···S, namely, S(1) and S(4) in complex **I** and S(3), S(4), S(5), and S(8) in complex **II**, form reliably stronger inner-cation covalent Au–S bonds (Table 2).

The $[FeCl_4]^-$ anions are localized at the right and left from the polymer chains (Figs. 2 and 5b). Anions **D** form short contacts only with centrosymmetrical cations **B** in the polymer chains. The Cl(1)···S(5) distances (3.531 Å) are somewhat shorter than the sum of

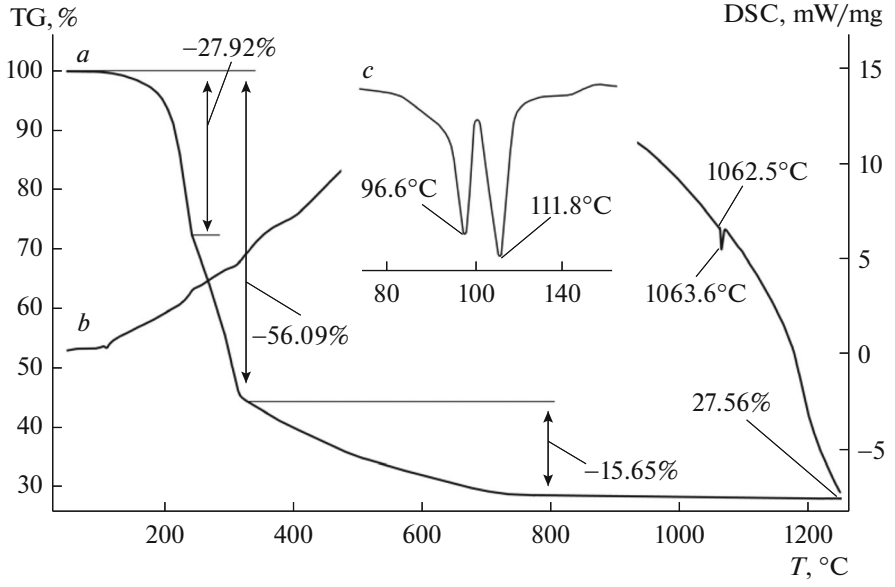

Fig. 6. (*a*) TG and (*b*) DSC curves for complex **I**. The low-temperature DSC region (*c*) was recorded in an aluminum crucible.

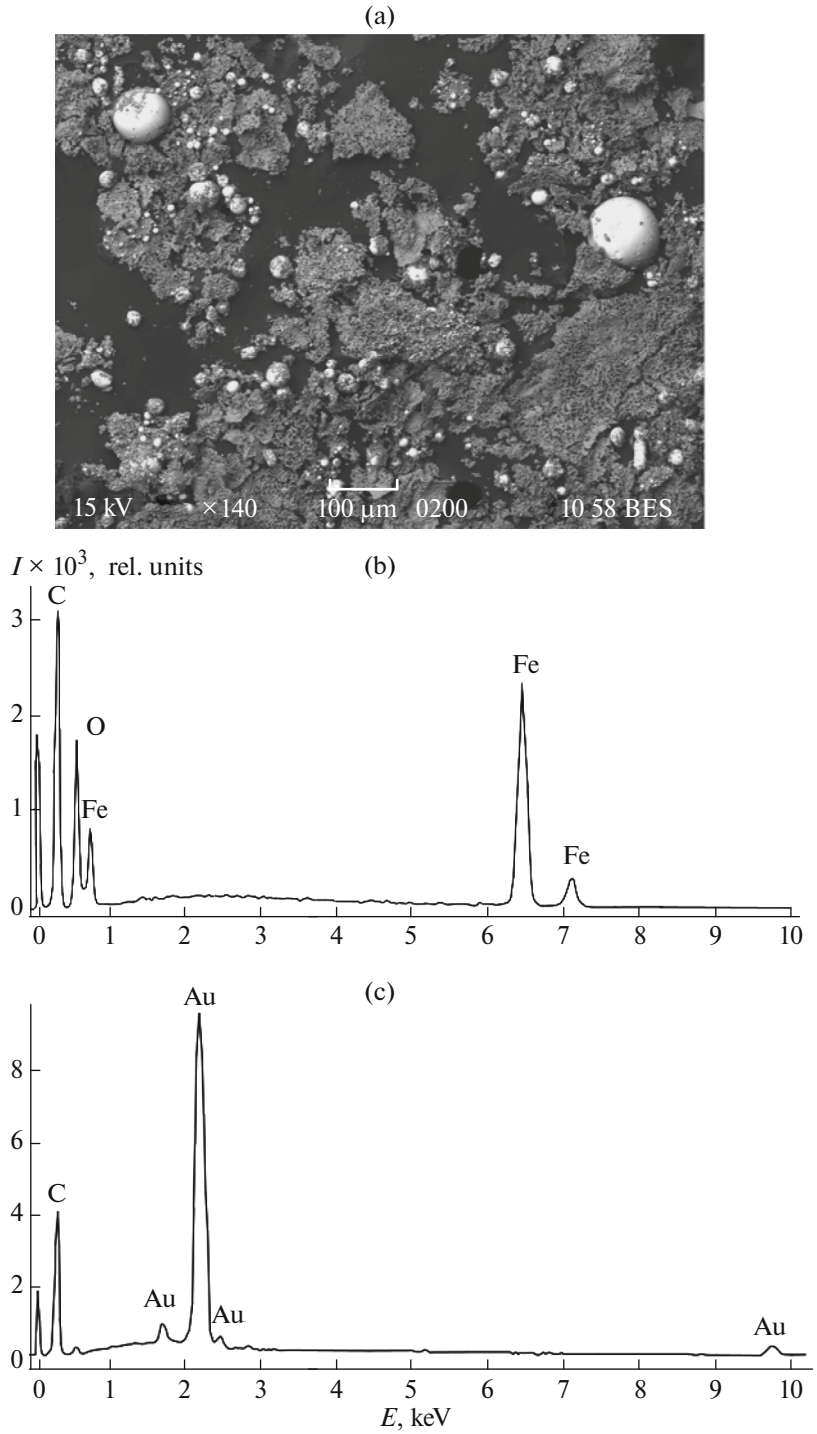

Fig. 7. (a) Slag particles with metallic gold balls after the thermal analysis of complex **I** and the energy dispersive spectra of (b) slag and (c) reduced gold.

the van der Waals radii of chlorine and sulfur atoms (3.55 Å) [31, 32]. Anions **E** are isolated.

The thermal behavior of compounds **I** and **II** was studied by the STA method using a combined detection of TG and DSC curves. Complexes **I** and **II** characterized by different structures of the alkyl substituents in the dithiocarbamate ligands demonstrate a similar character of thermal transformations. In particular, complex **I** exhibits thermal stability up to ~90°C (Fig. 6). The TG curve shows the two-stage process of mass loss (Fig. 6, *a*). The main mass loss equal to 56.09% of the initial value (the calculated

value is 55.29%) falls onto the first steeply-descending region of the TG curve (~90–330°C), indicating that the thermolysis proceeds simultaneously by the cation and anion with the reduction of gold(III) to metal and release of $FeCl_3$. The inflection point at 243.0°C divides this region of the TG curve into two approximately equal sections. The mass loss before the inflection point (27.92%) suggests that the initial stage of complex **I** defragmentation is related to the elimination of four alkyl groups in the Dtc ligands, escape of butylene molecules (calcd. 27.94%), and formation of the inorganic cation $[Au(S_2CNH_2)_2]^+$. An alternative variant can be the complete decomposition of one of the dibutyl dithiocarbamate ligands (calcd. 25.44%). At ~330°C the TG curve **I** reaches the region of gradual desorption of volatile thermolysis products (mainly due to the evaporation of released $FeCl_3$, b.p. 316°C [34]), which nearly completes to 800°C. However, the observed mass loss at this stage (15.65%) is substantially smaller than the calculated value (20.19%), whereas the residual mass at 1250°C (27.56%) exceeds the value calculated for reduced gold (24.52%) by 3.04%.

Let us consider reasons for the observed mass discrepancies in more detail. A red-brown substance with inclusions of fine yellow balls was observed on the bottom after the crucible was opened at the end of the process (1250°C). The energy dispersive spectra indicate the presence of iron and oxygen in the sintered slag mixture (Fig. 7b), whereas the lustrous yellow balls represent reduced metallic gold (Fig. 7c). Thus, some released $FeCl_3$ converts to Fe_2O_3 due to an oxygen impurity in argon. The calculations of the TG curve show that ~30% of iron in complex **I** convert to Fe_2O_3.

When using corundum crucibles, the DSC curve exhibits no significant endotherms in the low-temperature region (Fig. 6, *b*) and, hence, additional recording was carried out in aluminum crucibles (Fig. 6, *c*). In this case, the DSC curve has two pronounced endotherms with extremes at 96.6 and 111.8°C (the extrapolated temperatures are 91.3 and 109.3°C, respectively). The first irreversible endotherm is caused by the transition of the substance to a more stable crystalline modification, and the second endotherm shows melting of the complex. A melting range of 107–108°C was established for complex **I** by the independent determination in a glass capillary. The endotherm in the high-temperature range is due to the melting of reduced gold particles: the extrapolated melting point is 1062.5°C.

ACKNOWLEDGMENTS

This work was supported in part by the Presidium of the Far East Branch of the Russian Academy of Sciences (project no. 15-I-3-001) and the Ministry of Education and Science of the Russian Federation (project no. 1452.2014/9).

REFERENCES

1. Grekova, A.V., Ivanchenko, P.A., and Seifullina, I.I., *Vopr. Khim. Khim. Tekhnol.*, 2012, no. 1, p. 42.
2. Srinivasan, N., Thirumaran, S., and Ciattini, S., *J. Mol. Struct.*, 2014, vol. 1076, p. 382.
3. Srinivasan, N. and Thirumaran, S., *Comp. Rend. Chim.*, 2014, vol. 17, no. 9, p. 964.
4. Rani, P.J., Thirumaran, S., and Ciattini, S., *Spectrochim. Acta, Part A*, 2015, vol. 137, p. 1164.
5. Saravanan, M., Ramalingam, K., Bocelli, G., and Olla, R., *Appl. Organomet. Chem.*, 2004, vol. 18, no. 2, p. 103.
6. Manohar, A., Ramalingam, K., and Karpagavel, K., *Int. J. ChemTech. Res.*, 2014, vol. 6, no. 5, p. 2620.
7. Mansour, M.A., Connick, W.B., Lachicotte, R.J., et al., *J. Am. Chem. Soc.*, 1998, vol. 120, no. 6, p. 1329.
8. Han, S., Jung, O.-S., and Lee, Y.-A., *Transition Met. Chem.*, 2011, vol. 36, no. 7, p. 691.
9. Pitchaimani, P., Lo, K.M., and Elango, K.P., *Polyhedron*, 2015, vol. 93, p. 8.
10. Vanin, A.F., Bevers, L.M., Mikoyan, V.D., et al., *Nitric Oxide*, 2007, vol. 16, no. 1, p. 71.
11. Santos, K., Dinelli, L.R., Bogado, A.L., et al., *Inorg. Chim. Acta*, 2015, vol. 429, p. 237.
12. Ferreira, I.P., De Lima, G.M., Paniago, E.B., et al., *Eur. J. Med. Chem.*, 2012, vol. 58, p. 493.
13. De Lima, G.M., Menezes, D.C., Cavalcanti, C.A., et al., *J. Mol. Struct.*, 2011, vol. 988, nos. 1–3, p. 1.
14. Ronconi, L., Giovagnini, L., Marzano, C., et al., *Inorg. Chem.*, 2005, vol. 44, no. 6, p. 1867.
15. Ronconi, L., Marzano, C., Zanello, P., et al., *J. Med. Chem.*, 2006, vol. 49, no. 5, p. 1648.
16. Hogarth, G., *Mini-Rev. Med. Chem.*, 2012, vol. 12, no. 12, p. 1202.
17. Rodina, T.A., Ivanov, A.V., Gerasimenko, A.V., et al., *Polyhedron*, 2012, vol. 40, no. 1, p. 53.
18. Loseva, O.V., Rodina, T.A., and Ivanov, A.V., *Russ. J. Coord. Chem.*, 2013, vol. 39, no. 6, p. 463.
19. Ivanov, A.V., Rodina, T.A., and Loseva, O.V., *Russ. J. Coord. Chem.*, 2014, vol. 40, no. 12, p. 875.
20. Rodina, T.A., Loseva, O.V., Gerasimenko, A.V., and Ivanov, A.V., *Russ. J. Inorg. Chem.*, 2013, vol. 58, no. 9, p. 1104.
21. Ivanov, A.V., Loseva, O.V., Rodina, T.A., et al., *Russ. J. Inorg. Chem.*, 2014, vol. 59, no. 8, p. 807.
22. Loseva, O.V. and Ivanov, A.V., *Russ. J. Inorg. Chem.*, 2014, vol. 59, no. 12, p. 1491.
23. Loseva, O.V., Rodina, T.A., Smolentsev, A.I., and Ivanov, A.V., *J. Struct. Chem.*, 2014, vol. 55, no. 5, p. 901.
24. Zaeva, A.S., Ivanov, A.V., Gerasimenko, A.V., and Sergienko, V.I., *Russ. J. Inorg. Chem.*, 2015, vol. 60, no. 2, p. 203.
25. Zaeva, A.S., Ivanov, A.V., and Gerasimenko, A.V., *Russ. J. Coord. Chem.*, 2015, vol. 41, no. 10, p. 644.

26. Ivanov, A.V., Bredyuk, O.A., Loseva, O.V., and Rodina, T.A., *Russ. J. Coord. Chem.*, 2015, vol. 41, no. 2, p. 108.

27. Byr'ko, V.M., *Ditiokarbamaty* (Dithiocarbamates), Moscow: Nauka, 1984.

28. *APEX2*, Madison: Bruker AXS, 2010.

29. *SAINT*, Madison: Bruker AXS, 2010.

30. Sheldrick, G.M., *Acta Crystallogr., Sect. A*: *Found. Crystallogr.*, 2008, vol. 64, no. 1, p. 112.

31. Pauling, L., *The Nature of the Chemical Bond and the Structure of Molecules and Crystals*, London: Cornell Univ. Press, 1960.

32. Bondi, A., *J. Phys. Chem.*, 1966, vol. 70, no. 9, p. 3006.

33. Alcock, N.W., *Adv. Inorg. Chem. Radiochem.*, 1972, vol. 15, no. 1, p. 1.

34. Lidin, R.A., Andreeva, L.L., and Molochko, V.A., *Spravochnik po neorganicheskoi khimii* (Handbook in Inorganic Chemistry), Moscow: Khimiya, 1987.

Translated by E. Yablonskaya